PCCP
Physical Chemistry Chemical Physics

Accepted Manuscript

This article can be cited before page numbers have been issued, to do this please use: S. Barik, E. Livshits, R. Baer and D. Strasser, *Phys. Chem. Chem. Phys.*, 2026, DOI: 10.1039/D6CP00331A.

ROYAL SOCIETY OF CHEMISTRY

rsc.li/pccp

View Article Online
DOI: 10.1039/D6CP00331A

ARTICLE

Non-adiabatic Origin of Roaming OH Dynamics in the Formic Acid Dimer Dication

Received 00th January 20xx,
Accepted 00th January 20xx

DOI: 10.1039/x0xx00000x

Saroj Barik [a¶], Ester Livshits [a,b¶], Roi Baer [a,b*] and Daniel Strasser [a*]

Ionization of molecular clusters can trigger chemical reactions and drive chemical evolution even at very low temperatures, influencing chemistry in interstellar, atmospheric, and planetary environments exposed to ionizing radiation. To investigate such processes involving the dissociation of both intramolecular and intermolecular bonds under controlled conditions, we examined the dynamics of the formic acid (FA) dimer dication in an ultrafast extreme-ultraviolet (EUV) pump and near-infrared (NIR) probe experiment, combined with ab initio molecular dynamics simulations. The dissociation of the intermolecular bond and formation of the two-body $FA^+ + FA^+$ channel could be explained by ground-state dynamics, whereas the three-body breakup channels required a more detailed description. We developed a simplified dimer model for the breakup process that enabled carrying out non-adiabatic molecular dynamics simulations on excited-state CASPT2 potential energy surfaces that capture intermolecular as well as intramolecular dynamics. The simulations showed that soon after the dimer dissociation and non-adiabatic decay to the ground electronic state, a roaming-OH mechanism develops, accounting for the observed kinetic-energy-release distributions and momentum correlations in the $FA^+ + CHO^+ + OH$, and $FA^+ + H_2O^+ + CO$ three-body breakup channels. The simplified modeling approach may serve as a practical framework for studying excited-state dynamics in molecular dimer and cluster breakup processes.

Introduction

Ionization induced molecular dynamics have profound implications on the chemical evolution of interstellar medium and planetary atmosphere.[1–8] It can also initiate radiation damage processes in biological and materials systems.[9–12] Furthermore, ionization of molecular clusters can also be a powerful drive for chemical evolution and formation of new bonds in dilute and cold environments. For example, formation of aromatic bonds in ionization of acetylene clusters,[2] and peptide-bond formation on excited protonated serine dimer ions.[1] Ionization of symmetric dimer systems can result in symmetry-breaking dynamics due to asymmetric charge distributions in the ionized dimer.[3,13] The role of symmetry-breaking underscores a long-debated question about the sequential versus concerted proton-transfer dynamics in dual hydrogen bounded dimers, which are model systems for studies of radiation damage to DNA base pairs.[14–26] One of the simplest examples of a dual hydrogen-bonded system is the formic acid (FA) dimer.[27] Our recent study[13] combined ab initio molecular dynamics (AIMD) simulations with time-resolved ultrafast EUV pump–near-IR probe experiments to investigate its ionization-induced cation evolution, revealed proton transfer on both ultrafast, sub-picosecond time scale, as well as much slower dynamics ultimately forming the protonated monomer FAH^+.

In planetary ionospheres and in the interstellar medium, abundant ionizing radiation can induce double ionization, triggering new reaction mechanisms in which Coulomb explosion (CE) often serves as the dominant pathway. Yet, in certain molecular systems, CE cannot occur directly and instead requires preceding structural rearrangements. For example, in the double ionization of some organic species leading to H_3^+ formation, CE is facilitated by the roaming of a neutral H_2 fragment that subsequently drives ultrafast (~100 fs) electron- or proton-transfer processes.[28–37] Moiety roaming, a widespread phenomenon following photoexcitation or photoionization, frequently gives rise to unexpected reaction products. In such cases, prolonged roaming of hydrogen atoms[38–43] or even heavier molecular fragments[44–56] can result in the formation of new bonds far from the initial location of the roaming moiety within the parent molecule.

The formic acid (FA) dimer has also served as a benchmark system for studying double ionization and Coulomb explosion in dual hydrogen-bonded complexes. These processes have been investigated using both intense laser fields and electron-impact ionization.[57–59] In particular, Zhou et al. reported ultrafast intermolecular charge transfer induced sequential dissociation dynamics of the dimer, followed by cleavage of C–H and C–O bonds, leading to complex fragmentation patterns of the FA_2^{2+} dimer dication formed upon electron-impact ionization.[57]

[a] Institute of Chemistry, The Hebrew University of Jerusalem, Jerusalem 9190401, Israel.
[b] Fritz Haber Research Center for Molecular Dynamics, The Hebrew University of Jerusalem, Jerusalem 9190401, Israel.
* emails: strasser@huji.ac.il, roi.baer@mail.huji.ac. il
¶ These authors contributed equally to this work
Supplementary Information available: [details of any supplementary information available should be included here]. See DOI: 10.1039/x0xx00000x

View Article Online
DOI: 10.1039/D6CP00731F

Here, we report on the dynamics of the formic acid dimer dication (FA_2^{2+}) produced by double-ionization with an ultrashort EUV pulse and probed by a time-delayed near-IR pulse. Coincidence 3D imaging measurements of the ionic products, combined with non-adiabatic ab initio molecular dynamics simulations on the ground and excited states of the dication revealed the non-adiabatic origin of OH roaming dynamics that facilitate the measured $FA^+ + OH + CHO^+$ and $FA^+ + H_2O^+ + CO$ three-body product channels.

Results and discussion

Ionization of a molecular beam containing both FA monomers and dimers with broadband ultrashort EUV pulses produces multiple dissociative ionization and Coulomb explosion product channels.[13] Three-dimensional coincidence imaging enables identification of ions originating from single-photon double-ionization of FA dimers.[29,30,60–63] The FA_2^{2+} dication KER spectra, measured for the only two-body fragmentation product channel, $FA^+ + FA^+$, and for three additional three-body channels, are shown as black lines in the four panels of Fig. 1. Panel (a) displays a narrow KER distribution peaking near 4 eV, with a total $FA^+ + FA^+$ coincidences yield of approximately 5% of all the measured FA_2^{2+} decays. The observed peak lies slightly higher than the ~3.6 eV reported for intense-laser ionization of the FA dimer.[59] This result is consistent with other studies showing that single-photon double ionization with EUV photons can produce higher KER values than sequential ionization in intense laser fields.[60,64–66]

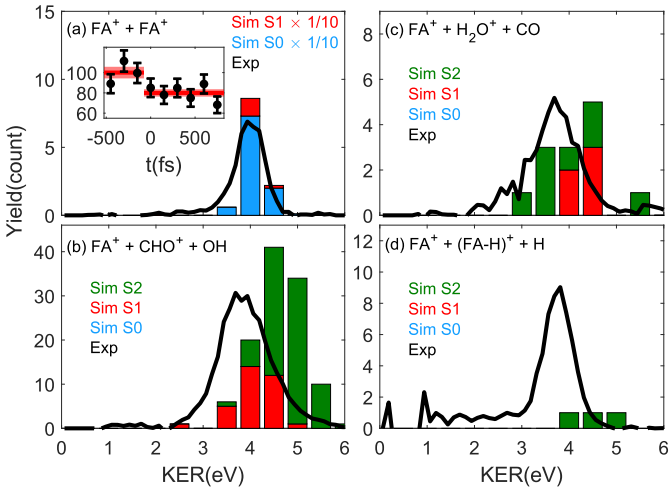

Figure 1: Comparison of the measured (black lines) and simulated KER spectra of the two-body and three-body breakup channels of the FA dimer dication. (a) $FA^+ + FA^+$, inset showing the relative channel yield dependence on pump-probe delay (b) $FA^+ + CHO^+ + OH$, (c) $FA^+ + H_2O^+ + CO$, and (d) $FA^+ + (FA\text{-}H)^+ + H$. Blue, red and green bars show simulated results from the S0, S1 and S2 states of FA_2^{2+} immediately after ionization. Experimental yields are in counts per 24 h acquisition time; simulated yields indicate the number of breakup trajectories (out of 100 per initial state) falling into each KER bin. The simulated yields in panel (a) are multiplied by factor 1/10 to match with experimental yield scale.

Our experimental measurements can be directly compared with simulated dynamics initiated on the low-lying excited states of the dication, produced by single-photon double ionization with a broadband ultrashort EUV pulse.[60] Accurate modeling of the FA_2^{2+} excited-state dynamics requires high-level quantum-chemical methods such as CASPT2, but for molecular clusters this approach is typically far too costly for generating a representative ensemble of molecular-dynamics trajectories. It can, however, be applied to single-point FA_2^{2+} calculations at a limited set of initial geometries near the Franck–Condon region. These calculations showed that immediately after double ionization, the system exhibits an initially symmetric charge separation. One hole is localized on the carbon atom of each monomer both for the dication ground state and for the low-lying excited electronic states. The two holes do not overlap spatially, and the energy splittings between the corresponding singlet and triplet eigenstates are very small (0.01–0.05 eV; for details, see SI). Together, these observations indicate that the intermonomer coupling is predominantly electrostatic and motivate an approximate modelling strategy in which one FA^+ monomer is treated quantum-mechanically, whereas the second monomer is represented as a movable point mass and charge. This approach made it possible to simulate high-level non-adiabatic dynamics on the three lowest electronic states: the ground state S0 and the two lowest excited states S1 and S2. In all three states, the explicit monomers are *in a doublet spin state. Fig. 2 shows snapshots of simulated FA dimer geometries, indicating the position of the 46 amu ion that is placed at the position of the central carbon atom of one of the FA monomers. The principal approximation in this model is the neglect of hydrogen bonding between the monomers, which can lead to differences in the energetics of the ground state and the two excited states. Using this quantum-chemical model, we performed non-adiabatic ab initio molecular-dynamics (NA-AIMD) simulations in which both the explicit monomer cation and the movable charge representing the partner monomer were included. Further computational details and checks of the model validity, including simulations of FA^+ monomers without a point charge, are provided in the SI and Methods section.

The simulated KER spectrum of the two-body breakup channel is shown in Figure 1a. It exhibits a narrow distribution peaking at 4 eV, in good agreement with the experimental data. The blue bars represent contributions from simulated trajectories on the S0 potential surface of the explicit monomer cation. All 100 S0 trajectories led to the two-body $FA^+ + FA^+$ dissociation channel. This was seen for the CASPT2 trajectories in the simple monomer model and also for DFT simulations of the triplet FA_2^{2+} ground state dynamics, where both monomers were fully represented. DFT calculations of the singlet ground state dynamics were discarded because of their non-single-determinant nature. Using NA-AIMD, we find that dynamics on the first excited state (S1) contribute only weakly to this two-body $FA^+ + FA^+$ channel, as indicated by the red bars in Figure 1a.

Journal Name ARTICLE

The inset in Figure 1a shows the measured effect of introducing a time-resolved near-IR probe on the ionization-induced dynamics. For the two-body $FA^+ + FA^+$ product channel, the time-delayed probe reduced the channel yield by about 20%. We attributed the reduced yield to enhanced electronic excitation of the dication by the near-IR pulse, thus supporting the theoretical prediction that the two-body channel originates primarily from ground-state dynamics.

The dominant three-body breakup channel (33% of all dication fragmentation events) is $FA^+ + CHO^+ + OH$, exhibits breakup of the intramolecular C-O bond in addition to the dimer dissociation. Its experimental KER distribution, shown in Figure 1b, peaks at 3.9eV and is markedly broader than that of the two-body channel. The simulations showed that this channel is obtained only for dynamics initiated on excited electronic states (S1 and S2) with a broad distribution similar to that of the experiment. Trajectories initiated on S1 reproduce the experimental KER distribution well, whereas those from S2 peak ~0.9 eV higher. Consequently, the total simulated distribution (S1 + S2) is pulled toward higher KER. This discrepancy likely arises from our assumption of equal initial populations for S1 and S2 (whereas double-ionization by the EUV pulse may favour S1) and/or from the reduced-dimensionality model, in which one FA monomer is treated as a movable point charge and thus may underestimate the dissipation of excess energy into its internal vibrational modes.

Dissociation of the C-O bond can also be accompanied by additional structural rearrangement and formation of the H_2O^+ product. The KER distribution of the $FA^+ + H_2O^+ + CO$ channel peaks at 3.8 eV and is similarly broad, though ~10 times weaker in yield compared with the $FA^+ + CHO^+ + OH$ channel in Figure 1b. Simulations indicate that this pathway likewise requires population of the excited states. The relative calculated yields of these three-body channels closely follow the experimental ones. This stands in contrast to the overestimated two-body breakup simulated in Figure 1a, which must be scaled by 1/10 to match the average number of $FA^+ + FA^+$ events per 24h measurement time.

In our earlier single-photon double ionization studies in methanol, we found uniform population of the low-lying singlet dication states.[60] However, the strong dominance of three-body breakup channels indicates that double ionization of the formic acid dimer by the EUV pulse preferentially populates excited dication states rather than the ground state. This can be explained by a mechanism in which one monomer is initially doubly-ionized, followed by ultrafast intermolecular charge transfer,[57] or by intermolecular Coulombic decay (ICD)[58,67] following an initial single-ionization of an inner level by the EUV pulse. These electronic decay processes typically occur on a fs or sub-fs timescale, effectively setting the "time zero" for subsequent nuclear dynamics before any significant structural rearrangement can occur. The rapid transition to excited states accounts for the relatively low yield of the two-body breakup channel, which the current model attributes mainly to ground-state dynamics.

The last three-body breakup channel exhibits H atom ejection from one of the dissociating monomers. Figure 1d shows the measured KER spectrum of the $FA^+ + (FA\text{-}H)^+ + H$ channel, exhibiting a narrow distribution peaking at ~3.8 eV, similar to the two-body channel. This channel was measured with similar yields as the two-body channel, nevertheless, it occurred in only 3 simulated trajectories on the S2 excited state. Zhou et al reported the same channel in electron-impact double ionization experiments and attributed it to sequential dissociation of the C-H bond on one of the FA^+ monomers following the dimer breakup.[57] To account for the excess excitation of electronic degrees of freedom and reproduce the C-H dissociation, Zhou et al performed theoretical ground-state simulations, including addition of 5.44 eV vibrational energy to the FA_2^{2+}.[57] The S2 state lies only ~3.2eV above the dication ground state, it is therefore possible that the main contribution to H dissociation is associated with higher lying potentials that were not considered here. Higher lying potentials are also likely to be involved in the observed four-body breakup channels. For example, the prominent $(FA\text{-}H)^+ + H + CHO^+ + OH$ channel that involves dissociation of both FA monomers. See SI for the complete branching ratios of all the measured CE channels.

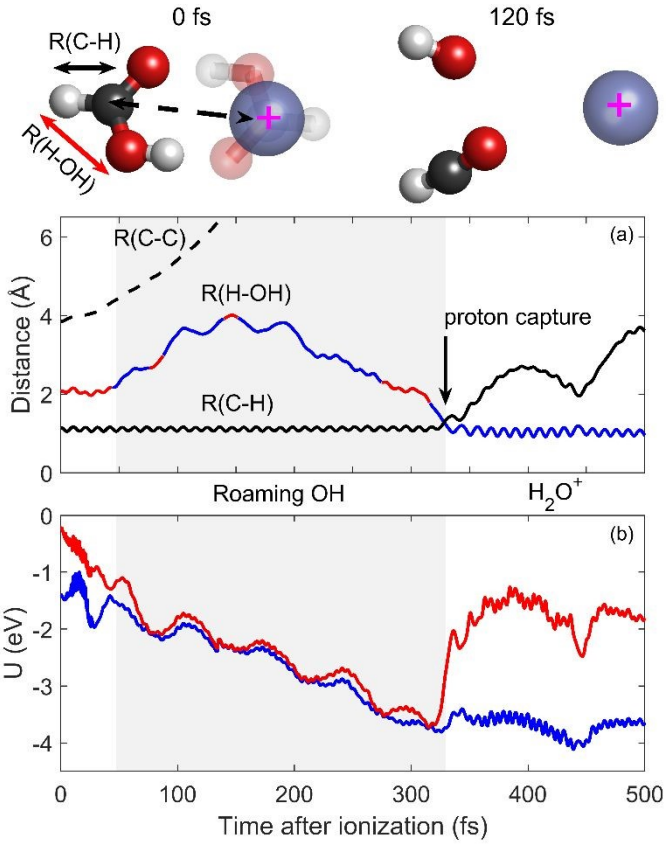

Figure 2: A typical H_2O-forming NA-AIMD trajectory that is initiated on the S_1 state of the dimer dication. The initial FA_2^{2+} geometry at 0 fs and 120 fs after ionisation are shown, where one of the FA^+ molecules is modelled with an equivalent 46 amu cation. (a) shows selected atomic distances as a function of time after ionization: solid and dashed black curves show the C-H and C-C distances respectively. Color-coded curve shows the H-OH distance, and its colour indicates the instantaneous electronic adiabatic state, with S1 represented by red and S0 by blue. (b) shows the S1 (in red) and S0 (in blue) potential energies along the same trajectory. Shaded region indicates the OH roaming time until

View Article Online
DOI: 10.1039/D6CP00331A

the formation of the H_2O^+ product by proton capture and its dissociation from the CO moiety.

The observed H_2O^+ products indicate a particularly non-trivial dissociation mechanism. Earlier studies of intense laser ionization of the FA monomer reported H_2O^+ formation and attributed it to the migration of the H atom from the C atom to the OH.[68] Nevertheless, its production in FA dimer ionization was not considered in the earlier experimental and theoretical studies.[57–59] One can tentatively consider several mechanisms that could form H_2O^+, starting from the initial geometry in which the two H atoms are separately situated in the CH and the OH moieties. An H-migration mechanism can be proposed, conversely, the heavier OH moiety can migrate towards the H atom on the other side of the FA monomer.[45–48,68] Figure 2 shows a typical H_2O^+ forming trajectory that was initiated on the S1 state. The dashed line in Figure 2a shows the simulated C-C distance (represented by the distance between the carbon atom of the explicit monomer and the position of the movable charge) that exhibits a direct ultrafast dissociation of the FA_2^{2+} dimer. In contrast, the C-H bond, indicated by the full black line, remains stable at ~1 Å, until a secondary dissociation that occurred ~330 fs time after ionization. The mechanism becomes clear when we consider the H-OH distance as a function of time after ionization, indicated by the color-coded curve. Initially on the S1 state, the H-OH distance remains stable at ~2 Å, reflecting the distance between the OH moiety and the second H that is bound to the carbon in the neutral FA monomer. After the dimer dissociation is well on its way, at ~44 fs, we observe a non-adiabatic transition from the S1 state to the S0 ground state, labelled respectively by red and blue line colour. As seen in Figure 2b, at that time, the S1 and S0 potentials, pass very close to a conical intersection that facilitates the non-adiabatic transition. On S0, the H-OH distance grows, as can be seen in Fig. 2 showing the FA_2^+ geometry snapshot taken 120 fs after ionization. The H-OH distance exhibits oscillations on a ~40fs time scale as the OH moiety roams around the monomer until it reaches the H atom on the other side. During the OH roaming, S1 and S0 become nearly degenerate, as the spin direction of the OH radical does not affect the potential of the distant CHO^+. However, as the OH captures a proton and dissociates, the degeneracy is lifted and the H-OH distance exhibits vibrational oscillations around the characteristic length of ~1 Å of H_2O^+'s OH bond.[69] The supplementary video file shows a molecular dynamics movie of this typical trajectory, clearly exhibiting roaming OH dynamics. This scenario concerning the onset of roaming is typical also for the dynamics initiated on the S2 state. In both initially excited states, the secondary dissociation of the H_2O^+ product occurred at long, up to 1ps times after ionization. More details about the simulated ensemble are provided in the SI.

When considering the combined yield of all three-body and four-body C-O bond breaking channels, we observed (as shown in the SI) few percent enhancement for positive probe delays, further supporting the theoretical prediction that the intermolecular fragmentation originates from excited state dynamics. Additional time-resolved insight can be obtained by comparing the measured and simulated momentum correlations of the three-body breakup events[70] shown in Figure

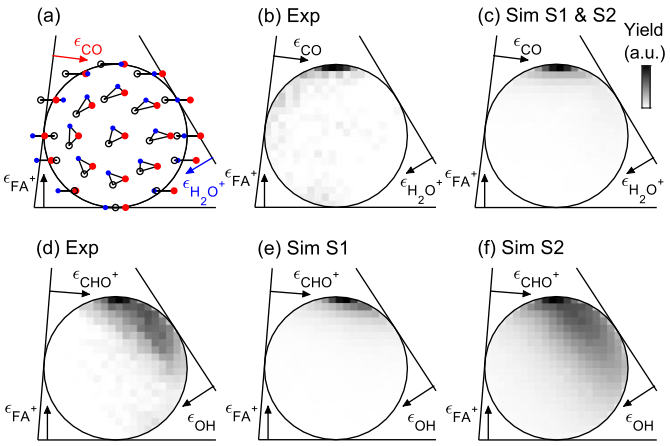

Figure 3: The 3-body momentum correlations for the $FA^+ + CHO^+ + OH$, and $FA^+ + H_2O^+ + CO$ channels. (a) Shows the mapping of $FA^+ + H_2O^+ + CO$ momentum correlations on to the mass scaled Dalitz plot representation. (b) and (c) Show respectively the measured and simulated correlations of the $FA^+ + H_2O^+ + CO$ channel. (d) Shows the measured correlations of the $FA^+ + CHO^+ + OH$ channel, while (e) and (f) show the simulated correlations for trajectories of the same channel initiated on the S1 and S2 states respectively.

3, where three-body momentum correlations are shown using the mass-scaled Dalitz plot representation. Figure 3a shows the mapping of momentum correlations for $FA^+ + H_2O^+ + CO$ dissociation events. Three correlated kinetic energy fraction axes ε_{FA+}, ε_{H2O+} and ε_{CO} are indicated, corresponding to the kinetic energy fraction of each fragment, scaled by the maximal possible fraction of each mass while conserving the total momentum in the center of mass frame. An uncorrelated three-body breakup would appear as a uniform distribution inside the unit circle. In contrast, the measured $FA^+ + H_2O^+ + CO$ events exhibit a highly correlated distribution that is shown in Figure 3b. In this channel, the FA^+ ions carry nearly the maximum possible kinetic energy while the remaining energy is randomly distributed between the H_2O^+ and CO products. This momentum correlation is typical for sequential dissociation,[30,62,71] in which an initial dissociation releases most of the available energy in a FA^+ - FA^+ Coulomb explosion. The secondary dissociation occurs after a sufficiently long time-delay, allowing for the loss of correlation between the angle of the H_2O^+ +CO dissociation vector and the direction of the intact FA^+ fragment. The same correlations can be seen in the simulated momentum correlations of the roaming OH dynamics resulting in the $FA^+ + H_2O^+ + CO$ channel that are shown in Figure 3c.

It is interesting to consider also the measured 3-body momentum correlations of the $FA^+ + CHO^+ + OH$ channel, shown in Figure 3d. Similar to the H_2O^+ formation channel, the distribution peaks at the maximal possible FA^+ energy fraction. However, for events with lower ε_{FA+}, the remaining energy is not randomly shared between CHO^+ and OH and is preferentially carried by the ε_{CHO+} product. This suggests a different scenario,

Journal Name ARTICLE

in which the second dissociation step can occur on a faster time scale that does not allow loss of correlation due to rotation of the C-O bond direction with respect to the direction of the dissociating FA^+ monomer. Furthermore, in such an early dissociation scenario, the ionic CHO^+ product can still gain additional kinetic energy due to the long-range repulsion from the FA^+ fragment. Figures 3e and 3f show the simulated momentum correlations for the FA^+ + CHO^+ + OH channel, initiated respectively on the S1 and S2 states. Trajectories starting on the S1 state reproduce the peak of the measured distribution attributed to long time delay between the intermolecular and intramolecular dissociation, while the S2 trajectories reproduce the correlated intermolecular and intramolecular bonds. Indeed, analysis of the simulated trajectory ensemble shown in the SI, demonstrates that roaming OH events initiated on S1 can culminate after up to 1ps time after ionization in release of the roaming neutral OH, rather than proton transfer and H_2O^+ formation. Most trajectories initiated on the S2 state exhibit a faster OH release within the first 100 fs, making it difficult to clearly assign the characteristic roaming OH motion.

Conclusions

In summary, the ultrafast intermolecular and intramolecular fragmentation dynamics of FA_2^{2+} dimers are studied by double-ionization in ultrafast EUV pump – near-IR probe experiments. 3D coincidence imaging measurements of the two-body and three-body breakup channels are directly compared with NA-AIMD simulations of excited state dynamics. The three-body momentum correlations reveal a rich roaming OH dynamics that are initiated after dissociation of the dimer and a non-adiabatic transition of initially electronically excited dication to the ground-electronic state on which the roaming occurs. The success of the simulations to predict channel-resolved kinetic energy release, H_2O^+ vs OH relative yields and momentum correlations in three-body breakup channels validates the chosen theoretical model that simplifies the cluster dynamics by considering one of the monomers as a point charge, while conserving the high-level electronic-structure calculation and non-adiabatic dynamics. We found that not only that the H_2O^+ formation is facilitated by roaming of the heavier OH, rather than the migration of a lighter H atom, but also that the ejection of neutral OH proceeds similarly via a roaming OH mechanism. Further studies are required to explore and validate the approach for simplified simulation of excited state dynamics in other molecular cluster systems, as well as to elucidate the role of roaming OH dynamics in other systems that exhibit competing H_2O^+ and OH production.

Methods

Experimental methods

The experimental setup and methodology have been described in the earlier work.[13,60–63] Molecular beam of formic acid dimer is produced in an effusive beam, formed by room temperature vapor pressure of FA is passed through a 200 micron aperture.[13] Ultrashort EUV pulses are produced by HHG in a semi-infinite Argon gas cell,[72,73] and are spatially filtered from the fundamental 800 nm laser of 35fs pulse. The broad-bandwidth EUV pulses, extending up to ~40 eV,[73] initiate dynamics on the ground and excited states of FA_2^{2+} dication by single-photon double-ionization, or by single-ionization of an inner electron followed by a nearly instantaneous ICD. The dynamics are probed by a time-delayed near-IR pulse, mildly focused to ~0.5 mm diameter and merged with the EUV pulse at the interaction region. The ionic products are accelerated to a time and position sensitive MCP detector, equipped with a phosphor anode. The timing information is read out by a fast scope and position information is acquired optically. Gain amplitude fluctuations were used to correlate time and position information.[74–77] 3D ion momenta are extracted from the ion recoil position in the detector plane and ion recoil in time-of-flight direction. In the three-body breakup channels, the neutral fragment momentum was calculated from the ions center of mass recoil in the lab frame.[60] Thus making it possible to measure channel resolved KER distributions and three body momentum correlations.[30,60,62] The reported data was acquired at a 1kHZ repetition rate over a period of 56 days, while scanning the near-IR delay in 50 fs steps.

Computational methods

NA-AIMD

The calculations were performed in three stages:

1. Thermalized initial conditions. A long-duration ab initio molecular-dynamics (AIMD) simulation of the neutral FA dimer was performed at 300 K using the DFT/BNL* functional (with range-separation parameter γ=0.417 a_0^{-1}, determined by tuning[78–80]) and the aug-cc-pVDZ basis set, as implemented in Q-Chem 5.4.[81] From this trajectory, 100 well-separated snapshots—chosen after the decay of temporal correlations—were extracted to represent a thermalized ensemble of initial geometries.

2. Replacement of one formic acid monomer by a dummy atom. For each initial condition, one formic acid molecule was replaced by a movable charge carrying the same net positive charge and mass as the monomer. The movable charge was positioned at the location of the carbon atom of the original acid molecule.

3. Nonadiabatic Ab Initio Molecular Dynamics (NA-AIMD). Each of the 100 configurations generated in Stage 2 were used to initiate a nonadiabatic molecular dynamics (MD) calculations on each of the three lowest-lying dicationic electronic states, yielding in a total of 300 trajectories. The nonadiabatic dynamics were treated using surface-hopping molecular dynamics trajectories[82] generated at the XMS-CASPT2/(13e,9o)/aug-cc-pVDZ/density-fitting level using the BAGEL electronic structure package.[83] The single-state single-reference (SS-SR) contraction scheme[84,85] was employed, with a vertical shift set to 0.2 E_h. BAGEL was interfaced with the Newton-X (v2.2)[86] to perform the surface-hopping NA-AIMD,[87] using a time step of 0.3 fs. Transitions were restricted to hops

between adjacent electronic states due to computational constraints. The ab initio dynamics were propagated for up to 1 ps, or until the interfragment velocities reached an asymptotic, monotonic regime. At this point, the residual long-range Coulomb repulsion was accounted for by propagating the centers of mass of the resulting cationic fragments using classical equations of motion.

Fully atomistic DFT AIMD reference simulations.

In addition to the NA-AIMD calculations, fully atomistic DFT AIMD simulations were carried out assuming a triplet ground electronic state, with both FA monomers explicitly represented. The same electronic structure package and DFT methodology described in stage 1 were employed. The simulations were initiated from the same 100 well-separated snapshots described in stage 1, and all trajectories were propagated for 1 ps.

Author contributions

Saroj Barik: Conceptualization, Data curation, Formal analysis, Investigation, Methodology, Software, Validation, Visualization, Writing – original draft, Writing – review & editing. Ester Livshits: Conceptualization, Data curation, Formal analysis, Investigation, Methodology, Software, Validation, Visualization, Writing – review & editing, Roi Baer: Conceptualization, Formal analysis, Funding acquisition, Investigation, Methodology, Project administration, Resources, Software, Supervision, Validation, Visualization, Writing – review & editing, Daniel Strasser: Conceptualization, Data curation, Formal analysis, Funding acquisition, Investigation, Methodology, Project administration, Resources, Software, Supervision, Validation, Visualization, Writing – original draft, Writing – review & editing

Conflicts of interest

There are no conflicts to declare.

Data availability

The data supporting this study are available within the main text and the supplementary information (SI).

Acknowledgements

The authors acknowledge the support from ISF grants 1153/23, and 2539/25 as well as support from the Minerva Center for Making Bonds by Fragmentation. S.B. acknowledges support provided by the Lady Davis Fellowship.

References

(1) Licht, O.; Barreiro-Lage, D.; Rousseau, P.; Giuliani, A.; Milosavljević, A. R.; Isaak, A.; Mastai, Y.; Albeck, A.; Singh, R.; Nguyen, V. T. T.; Nahon, L.; Martínez-Fernández, L.; Díaz-Tendero, S.; Toker, Y. Peptide Bond Formation in the Protonated Serine Dimer Following Vacuum UV Photon-Induced Excitation. *Angew. Chem. Int. Ed.* **2023**, *62* (15). https://doi.org/10.1002/anie.202218770.

(2) Stein, T.; Bandyopadhyay, B.; Troy, T. P.; Fang, Y.; Kostko, O.; Ahmed, M.; Head-Gordon, M. Ab Initio Dynamics and Photoionization Mass Spectrometry Reveal Ion-Molecule Pathways from Ionized Acetylene Clusters to Benzene Cation. *Proc. Natl. Acad. Sci. U. S. A.* **2017**, *114* (21), E4125–E4133. https://doi.org/10.1073/pnas.1616464114.

(3) Livshits, E.; Bittner, D. M.; Trost, F.; Meister, S.; Lindenblatt, H.; Treusch, R.; Gope, K.; Pfeifer, T.; Baer, R.; Moshammer, R.; Strasser, D. Symmetry-Breaking Dynamics of a Photoionized Carbon Dioxide Dimer. *Nat. Commun.* **2024**, *15* (1), 6322. https://doi.org/10.1038/s41467-024-50759-2.

(4) Londoño-Restrepo, J.; Gómez, S.; Quitián-Lara, H. M.; Fantuzzi, F.; Restrepo, A. More p, Please: What Drives the Formation of Unsaturated Molecules in the Interstellar Medium? *Chem. Sci.* **2025**, *16* (7), 3051–3065. https://doi.org/10.1039/d4sc07986h.

(5) Gatchell, M.; Delaunay, R.; D'Angelo, G.; Mika, A.; Kulyk, K.; Domaracka, A.; Rousseau, P.; Zettergren, H.; Huber, B. A.; Cederquist, H. Ion-Induced Molecular Growth in Clusters of Small Hydrocarbon Chains. *Physical Chemistry Chemical Physics* **2017**, *19* (30), 19665–19672. https://doi.org/10.1039/c7cp02090b.

(6) Ganguly, S.; Barreiro-Lage, D.; Walsh, N.; Oostenrijk, B.; Sorensen, S. L.; Díaz-Tendero, S.; Gisselbrecht, M. The Origin of Enhanced O2+ Production from Photoionized CO2 Clusters. *Commun. Chem.* **2022**, *5* (1). https://doi.org/10.1038/s42004-022-00629-z.

(7) Matsubara, T. Theoretical Insights into a Novel Ion-Ion Reaction of Methane in the Initial Stages of Hydrocarbon Growth in Space. *ACS Earth Space Chem.* **2024**. https://doi.org/10.1021/acsearthspacechem.4c00242.

(8) Daniely, A.; Wannenmacher, A.; Levy, N.; Sheffer, O.; Joseph, E.; Kostko, O.; Ahmed, M.; Stein, T. A Vacuum Ultraviolet Photoionization Mass Spectrometry and Density Functional Calculation Study of Formic Acid-Water Clusters. *Journal of Physical Chemistry A* **2024**, *128* (31), 6392–6401. https://doi.org/10.1021/acs.jpca.4c02875.

(9) Alizadeh, E.; Orlando, T. M.; Sanche, L. Biomolecular Damage Induced by Ionizing Radiation: The Direct and Indirect Effects of Low-Energy Electrons on DNA. *Annu. Rev. Phys. Chem.* **2015**, *66*, 379–398. https://doi.org/10.1146/annurev-physchem-040513-103605.

(10) Hergenhahn, U. Production of Low Kinetic Energy Electrons and Energetic Ion Pairs by Intermolecular Coulombic Decay. In *International Journal of Radiation Biology*; 2012; Vol. 88, pp 871–883. https://doi.org/10.3109/09553002.2012.698031.

(11) Yokoya, A.; Ito, T. Photon-Induced Auger Effect in Biological Systems: A Review. *International Journal of Radiation Biology*. Taylor and Francis Ltd August 3, 2017, pp 743–756. https://doi.org/10.1080/09553002.2017.1312670.

(12) Asmussen, J. D.; Abid, A. R.; Sundaralingam, A.; Bastian, B.; Sishodia, K.; De, S.; Ben Ltaief, L.; Krishnan, S.; Pedersen, H. B.; Mudrich, M. Secondary Ionization of Pyrimidine Nucleobases and Their Microhydrated Derivatives in Helium Nanodroplets. *Physical Chemistry Chemical Physics* **2023**, *25* (36), 24819–24828. https://doi.org/10.1039/d3cp02879h.

(13) Barik, S.; Livshits, E.; Baer, R.; Strasser, D. Ultrafast and Ultraslow Proton-Transfer Dynamics Induced by Formic Acid Dimer Ionization. *J. Phys. Chem. A* **2025**, *16*, 37. https://doi.org/10.1021/acs.jpca.5c02619.

(14) Schreier, W. J.; Gilch, P.; Zinth, W. Early Events of DNA Photodamage. *Annu. Rev. Phys. Chem.* **2015**, *66*, 497–519. https://doi.org/10.1146/annurev-physchem-040214-121821.

(15) Löwdin, P.-O. Proton Tunneling in DNA and Its Biological Implications. *Rev. Mod. Phys.* **1963**, *35* (3), 724–732. https://doi.org/10.1103/RevModPhys.35.724.

(16) WATSON, J. D.; CRICK, F. H. C. Molecular Structure of Nucleic Acids: A Structure for Deoxyribose Nucleic Acid. *Nature* **1953**, *171* (4356), 737–738. https://doi.org/10.1038/171737a0.

(17) Kim, Y. Direct Dynamics Calculation for the Double Proton Transfer in Formic Acid Dimer. *J. Am. Chem. Soc.* **1996**, *118* (6), 1522–1528. https://doi.org/10.1021/ja953175v.

(18) Ivanov, S. D.; Grant, I. M.; Marx, D. Quantum Free Energy Landscapes from Ab Initio Path Integral Metadynamics: Double Proton Transfer in the Formic Acid Dimer Is Concerted but Not Correlated. *Journal of Chemical Physics* **2015**, *143* (12). https://doi.org/10.1063/1.4931052.

(19) Ushiyama, H.; Takatsuka, K. Successive Mechanism of Double-Proton Transfer in Formic Acid Dimer: A Classical Study. *Journal of Chemical Physics* **2001**, *115* (13), 5903–5912. https://doi.org/10.1063/1.1398090.

(20) Kohanoff, J.; Koval, S.; Estrin, D. A.; Laria, D.; Abashkin, Y. Concertedness and Solvent Effects in Multiple Proton Transfer Reactions: The Formic Acid Dimer in Solution. *Journal of Chemical Physics* **2000**, *112* (21), 9498–9508. https://doi.org/10.1063/1.481585. DOI: 10.1039/D6CP00331A

(21) Tachikawa, H. Proton Transfer vs Complex Formation Channels in Ionized Formic Acid Dimer: A Direct Ab Initio Molecular Dynamics Study. *Journal of Physical Chemistry A* **2020**, *124* (16), 3048–3054. https://doi.org/10.1021/acs.jpca.0c01729.

(22) Li, W.; Evangelisti, L.; Gou, Q.; Caminati, W.; Meyer, R. The Barrier to Proton Transfer in the Dimer of Formic Acid: A Pure Rotational Study. *Angewandte Chemie* **2019**, *131* (3), 869–875. https://doi.org/10.1002/ange.201812754.

(23) Sutton, S. F.; Rotteger, C. H.; Jarman, C. K.; Tarakeshwar, P.; Sayres, S. G. Ultrafast Proton Transfer and Contact Ion-Pair Formation in Formic Acid Clusters. *Journal of Physical Chemistry Letters* **2023**, *14* (37), 8306–8311. https://doi.org/10.1021/acs.jpclett.3c01654.

(24) Mackeprang, K.; Xu, Z. H.; Maroun, Z.; Meuwly, M.; Kjaergaard, H. G. Spectroscopy and Dynamics of Double Proton Transfer in Formic Acid Dimer. *Physical Chemistry Chemical Physics* **2016**, *18* (35), 24654–24662. https://doi.org/10.1039/c6cp03462d.

(25) Sekiya, H.; Sakota, K. Excited-State Double-Proton Transfer in a Model DNA Base Pair: Resolution for Stepwise and Concerted Mechanism Controversy in the 7-Azaindole Dimer Revealed by Frequency- and Time-Resolved Spectroscopy. *Journal of Photochemistry and Photobiology C: Photochemistry Reviews*. June 2008, pp 81–91. https://doi.org/10.1016/j.jphotochemrev.2008.04.001.

(26) Crespo-Otero, R.; Kungwan, N.; Barbatti, M. Stepwise Double Excited-State Proton Transfer Is Not Possible in 7-Azaindole Dimer. *Chem. Sci.* **2015**, *6* (10), 5762–5767. https://doi.org/10.1039/c5sc01902h.

(27) Farfán, P.; Echeverri, A.; Diaz, E.; Tapia, J. D.; Gómez, S.; Restrepo, A. Dimers of Formic Acid: Structures, Stability, and Double Proton Transfer. *Journal of Chemical Physics* **2017**, *147* (4). https://doi.org/10.1063/1.4985880.

(28) Livshits, E.; Luzon, I.; Gope, K.; Baer, R.; Strasser, D. Time-Resolving the Ultrafast H2 Roaming Chemistry and H3+ Formation Using Extreme-Ultraviolet Pulses. *Commun. Chem.* **2020**, *3* (1), 49. https://doi.org/10.1038/s42004-020-0294-1.

(29) Strasser, D.; Livshits, E.; Baer, R. Single-Photon Double-Ionisation Coulomb Explosion in Organic Molecules. *Int. Rev. Phys. Chem.* **2023**, *42* (1–4), 29–51. https://doi.org/10.1080/0144235X.2023.2450916.

(30) Gope, K.; Bittner, D. M.; Strasser, D. Sequential Mechanism in H 3 + Formation Dynamics on the Ethanol Dication . *Physical Chemistry Chemical Physics* **2023**, *25* (9), 6979–6986. https://doi.org/10.1039/d2cp03632k.

(31) Gope, K.; Livshits, E.; Bittner, D. M.; Baer, R.; Strasser, D. Two Pathways and an Isotope Effect in H3+ Formation Following Double Ionization of Methanol. *Natural Sciences* **2021**, *1* (2). https://doi.org/10.1002/ntls.10022.

(32) Gope, K.; Livshits, E.; Bittner, D. M.; Baer, R.; Strasser, D. An "Inverse" Harpoon Mechanism. *Sci. Adv.* **2022**, *8* (39), 8084. https://doi.org/10.1126/sciadv.abq8084.

(33) Mishra, D.; LaForge, A. C.; Gorman, L. M.; Díaz-Tendero, S.; Martín, F.; Berrah, N. Direct Tracking of H2 Roaming Reaction in Real Time. *Nat. Commun.* **2024**, *15* (1). https://doi.org/10.1038/s41467-024-49671-6.

(34) Ngai, A.; Hartweg, S.; Asmussen, J. D.; Bastian, B.; Bonanomi, M.; Callegari, C.; Danailov, M.; di Fraia, M.; Feifel, R.; Ganeshamandiram, S. D.; Krishnan, S.; LaForge, A.; Landmesser, F.; Ltaief, L. Ben; Michelbach, M.; Pal, N.; Plekan, O.; Rendler, N.; Raimondi, L.; Richter, F.; Scognamiglio, A.; Sixt, T.; Squibb, R. J.; Dulitz, K.; Stienkemeier, F.; Mudrich, M. -Roaming Dynamics in the Formation of Following Two-Photon Double Ionization of Ethanol and Aminoethanol. *Sci. Rep.* **2025**, *15* (1). https://doi.org/10.1038/s41598-024-84531-9.

(35) Ekanayake, N.; Severt, T.; Nairat, M.; Weingartz, N. P.; Farris, B. M.; Kaderiya, B.; Feizollah, P.; Jochim, B.; Ziaee, F.; Borne, K.; Raju P, K.; Carnes, K. D.; Rolles, D.; Rudenko, A.; Levine, B. G.; Jackson, J. E.; Ben-Itzhak, I.; Dantus, M. H2 Roaming Chemistry and the Formation of H3+ from Organic Molecules in Strong Laser Fields. *Nat. Commun.* **2018**, *9* (1). https://doi.org/10.1038/s41467-018-07577-0.

(36) Yoshikawa, K.; Kanno, M.; Xue, H.; Kishimoto, N.; Goto, S.; Ota, F.; Tamura, Y.; Trinter, F.; Fehre, K.; Kaiser, L.; Stindl, J.; Tsitsonis, D.; Schöffler, M.; Dörner, R.; Boll, R.; Erk, B.; Mazza, T.; Mullins, T.; Rivas, D. E.; Schmidt, P.; Usenko, S.; Meyer, M.; Wang, E.; Rolles, D.; Rudenko, A.; Kukk, E.; Jahnke, T.; Díaz-Tendero, S.; Martín, F.; Hatada, K.; Ueda, K. Time-Resolved Photoelectron Diffraction Imaging of Methanol Photodissociation Involving Molecular Hydrogen Ejection. *Physical Chemistry Chemical Physics* **2024**, *26* (38), 25118–25130. https://doi.org/10.1039/d4cp01015a.

(37) Wang, E.; Kling, N. G.; LaForge, A. C.; Obaid, R.; Pathak, S.; Bhattacharyya, S.; Meister, S.; Trost, F.; Lindenblatt, H.; Schoch, P.; Kübel, M.; Pfeifer, T.; Rudenko, A.; Díaz-Tendero, S.; Martín, F.; Moshammer, R.; Rolles, D.; Berrah, N. Ultrafast Roaming Mechanisms in Ethanol Probed by Intense Extreme Ultraviolet Free-Electron Laser Radiation: Electron Transfer versus Proton Transfer. *Journal of Physical Chemistry Letters* **2023**, *14* (18), 4372–4380. https://doi.org/10.1021/acs.jpclett.2c03764.

(38) Townsend, D.; Lahankar, S. A.; Lee, S. K.; Chambreau, S. D.; Suits, A. G.; Zhang, X.; Rheinecker, J.; Harding, L. B.; Bowman, J. M. The Roaming Atom: Straying from the Reaction Path in Formaldehyde Decomposition. *Science (1979).* **2004**, *306* (5699), 1158–1161. https://doi.org/10.1126/science.1104386.

(39) Suits, A. G. Roaming Atoms and Radicals: A New Mechanism in Molecular Dissociation. *Acc. Chem. Res.* **2008**, *41* (7), 873–881. https://doi.org/10.1021/ar8000734.

(40) Lahankar, S. A.; Chambreau, S. D.; Townsend, D.; Suits, F.; Farnum, J.; Zhang, X.; Bowman, J. M.; Suits, A. G. The Roaming Atom Pathway in Formaldehyde Decomposition. *Journal of Chemical Physics* **2006**, *125* (4). https://doi.org/10.1063/1.2202241.

(41) Fu, Y. L.; Bai, Y.; Han, Y. C.; Fu, B.; Zhang, D. H. Double-Roaming Dynamics in the H + C2H2→ H2+ C2H Reaction: Acetylene-Facilitated Roaming and Vinylidene-Facilitated Roaming. *Journal of Physical Chemistry Letters* **2021**, *12* (17), 4211–4217. https://doi.org/10.1021/acs.jpclett.1c01045.

(42) Bencsura, Á.; Lendvay, G. Bimolecular Reactions of Vibrationally Excited Molecules. Roaming Atom Mechanism at Low Kinetic Energies. *Journal of Physical Chemistry A* **2012**, *116* (18), 4445–4456. https://doi.org/10.1021/jp301243a.

(43) Endo, T.; Neville, S. P.; Wanie, V.; Beaulieu, S.; Qu, C.; Deschamps, J.; Lassonde, P.; Schmidt, B. E.; Fujise, H.; Fushitani, M.; Hishikawa, A.; Houston, P. L.; Bowman, J. M.; Schuurman, M. S.; Légaré, F.; Ibrahim, H. Capturing Roaming Molecular Fragments in Real Time. *Science (1979).* **2020**, *370* (6520), 1072–1077. https://doi.org/10.1126/science.abc2960.

(44) Severt, T.; Daugaard, D. R.; Townsend, T.; Ziaee, F.; Borne, K.; Bhattacharyya, S.; Carnes, K. D.; Rolles, D.; Rudenko, A.; Wells, E.; Ben-Itzhak, I. Two-Body Dissociation of Formic Acid Following Double Ionization by Ultrafast Laser Pulses. *Phys. Rev. A (Coll. Park).* **2022**, *105* (5). https://doi.org/10.1103/PhysRevA.105.053112.

(45) Maeda, S.; Taketsugu, T.; Morokuma, K. Automated Exploration of Photolytic Channels of HCOOH: Conformational Memory via Excited-State Roaming. *Journal of Physical Chemistry Letters* **2012**, *3* (14), 1900–1907. https://doi.org/10.1021/jz300728q.

(46) Ma, Y.; Liu, J.; Li, F.; Wang, F.; Kitsopoulos, T. N. Roaming Dynamics in the Photodissociation of Formic Acid at 230 Nm. *Journal of Physical Chemistry A* **2019**, *123* (17), 3672–3677. https://doi.org/10.1021/acs.jpca.9b00724.

(47) Lin, K. C.; Tso, C. J.; Kasai, T. Beyond the Rule of Transition State: Identification of Roaming Routes in Some Cases of Carbonyl Compounds. *Journal of the Chinese Chemical Society* **2021**, *68* (8), 1358–1378. https://doi.org/10.1002/jccs.202100039.

(48) Tso, C. J.; Kasai, T.; Lin, K. C. Roaming Dynamics and Conformational Memory in Photolysis of Formic Acid at 193 Nm Using Time-Resolved Fourier-Transform Infrared Emission Spectroscopy. *Sci. Rep.* **2020**, *10* (1). https://doi.org/10.1038/s41598-020-61642-7.

(49) Liu, T.; Elliott, S. N.; Zou, M.; Vansco, M. F.; Sojdak, C. A.; Markus, C. R.; Almeida, R.; Au, K.; Sheps, L.; Osborn, D. L.; Winiberg, F. A. F.; Percival, C. J.; Taatjes, C. A.; Caravan, R. L.; Klippenstein, S. J.; Lester, M. I. OH Roaming and Beyond in the Unimolecular Decay of the Methyl-Ethyl-Substituted Criegee Intermediate: Observations and Predictions. *J. Am. Chem. Soc.* **2023**, *145* (35), 19405–19420. https://doi.org/10.1021/jacs.3c07126.

(50) Klippenstein, S. J.; Elliott, S. N. OH Roaming during the Ozonolysis of α-Pinene: A New Route to Highly Oxygenated Molecules? *Journal of Physical Chemistry A* **2023**, *127* (50), 10647–10662. https://doi.org/10.1021/acs.jpca.3c05179.

(51) Del Mazo-Sevillano, P.; Aguado, A.; Jiménez, E.; Suleimanov, Y. V.; Roncero, O. Quantum Roaming in the Complex-Forming Mechanism of the Reactions of OH with Formaldehyde and Methanol at Low Temperature and Zero Pressure: A Ring Polymer Molecular Dynamics Approach. *Journal of Physical Chemistry Letters* **2019**, *10* (8), 1900–1907. https://doi.org/10.1021/acs.jpclett.9b00555.

(52) Li, Z.; Fu, Y.; Luo, Z.; Yang, S.; Wu, Y.; Wu, H.; Wu, G.; Zhang, W.; Fu, B.; Yuan, K.; Zhang, D.; Yang, X. Roaming in Highly Excited States: The Central Atom Elimination of Triatomic Molecule Decomposition. *Science (1979).* **2024**, *383* (6684), 746–750. https://doi.org/10.1126/science.adn3357.

(53) Kamarchik, E.; Koziol, L.; Reisler, H.; Bowman, J. M.; Krylov, A. I. Roaming Pathway Leading to Unexpected Water + Vinyl Products in C 2H4OH Dissociation. *Journal of Physical Chemistry Letters* **2010**, *1* (20), 3058–3065. https://doi.org/10.1021/jz1011884.

(54) Heazlewood, B. R.; Jordan, M. J. T.; Kable, S. H.; Selby, T. M.; Osborn, D. L.; Shepler, B. C.; Braams, B. J.; Bowman, J. M. Roaming Is the Dominant Mechanism for Molecular Products in Acetaldehyde Photodissociation. *Proceedings of the National Academy of Sciences* **2008**, *105* (35), 12719–12724. https://doi.org/10.1073/pnas.0802769105.

(55) Bejoy, N. B.; Roy Chowdhury, P.; Patwari, G. N. Modulating the Roaming Dynamics for the NO Release in Ortho-Nitrobenzenes. *Journal of Physical Chemistry Letters* **2023**, *14* (11), 2816–2822. https://doi.org/10.1021/acs.jpclett.3c00134.

(56) Matsubara, T. Dynamic Effects on the Ionization-Induced Reactions of Methyl Halides: Quantum Mechanical and Molecular Dynamics Studies. *Journal of Physical Chemistry A* **2023**, *127* (22), 4801–4814. https://doi.org/10.1021/acs.jpca.3c01669.

(57) Zhou, J.; Jia, S.; Hu, X.; Wang, E.; Xue, X.; Wu, Y.; Wang, J.; Dorn, A.; Ren, X. Intermolecular Charge Transfer Induced Fragmentation of Formic Acid Dimers. *Phys. Rev. Lett.* **2023**, *130* (23). https://doi.org/10.1103/PhysRevLett.130.233001.

(58) Zhou, J.; Jia, S.; Skitnevskaya, A. D.; Wang, E.; Hähnel, T.; Grigoricheva, E. K.; Xue, X.; Li, J. X.; Kuleff, A. I.; Dorn, A.; Ren, X. Concerted Double Hydrogen-Bond Breaking by Intermolecular Coulombic Decay in the Formic Acid Dimer. *Journal of Physical Chemistry Letters* **2022**, *13* (19), 4272–4279. https://doi.org/10.1021/acs.jpclett.2c00957.

(59) Hoshina, K.; Hagihara, H.; Tsuge, M. Double Ionization and Coulomb Explosion of the Formic Acid Dimer by Intense Near-Infrared Femtosecond Laser Pulses. *Journal of Physical Chemistry A* **2012**, *116* (2), 826–831. https://doi.org/10.1021/jp2111154.

(60) Luzon, I.; Livshits, E.; Gope, K.; Baer, R.; Strasser, D. Making Sense of Coulomb Explosion Imaging. *Journal of Physical Chemistry Letters* **2019**, *10* (6), 1361–1367. https://doi.org/10.1021/acs.jpclett.9b00576.

(61) Luzon, I.; Jagtap, K.; Livshits, E.; Lioubashevski, O.; Baer, R.; Strasser, D. Single-Photon Coulomb Explosion of Methanol Using Broad Bandwidth Ultrafast EUV Pulses. *Physical Chemistry Chemical Physics* **2017**, *19* (21), 13488–13495. https://doi.org/10.1039/c7cp00587c.

(62) Bittner, D. M.; Gope, K.; Livshits, E.; Baer, R.; Strasser, D. Sequential and Concerted C-C and C-O Bond Dissociation in the Coulomb Explosion of 2-Propanol. *Journal of Chemical Physics* **2022**, *157* (7). https://doi.org/10.1063/5.0098531.

(63) Bittner, D. M.; Gope, K.; Strasser, D. Time-Resolved Dissociative Ionization and Double Photoionization of CO2. *Journal of Chemical Physics* **2020**, *153* (19). https://doi.org/10.1063/5.0028812.

(64) Ekanayake, N.; Nairat, M.; Kaderiya, B.; Feizollah, P.; Jochim, B.; Severt, T.; Berry, B.; Pandiri, K. R.; Carnes, K. D.; Pathak, S.; Rolles, D.; Rudenko, A.; Ben-Itzhak, I.; Mancuso, C. A.; Fales, B. S.; Jackson, J. E.; Levine, B. G.; Dantus, M. Mechanisms and Time-Resolved Dynamics for Trihydrogen Cation (H3+) Formation from Organic Molecules in Strong Laser Fields. *Sci. Rep.* **2017**, *7* (1). https://doi.org/10.1038/s41598-017-04666-w.

(65) Xu, H.; Okino, T.; Kudou, T.; Yamanouchi, K.; Roither, S.; Kitzler, M.; Baltuska, A.; Chin, S. L. Effect of Laser Parameters on Ultrafast Hydrogen Migration in Methanol Studied by Coincidence Momentum Imaging. In *Journal of Physical Chemistry A*; 2012; Vol. 116, pp 2686–2690. https://doi.org/10.1021/jp207483y.

(66) Ando, T.; Shimamoto, A.; Miura, S.; Iwasaki, A.; Nakai, K.; Yamanouchi, K. Coherent Vibrations in Methanol Cation Probed by Periodic H3+ Ejection after Double Ionization. *Commun. Chem.* **2018**, *1* (1). https://doi.org/10.1038/s42004-017-0006-7.

(67) Cederbaum, L. S.; Zobeley, J.; Tarantelli, F. Giant Intermolecular Decay and Fragmentation of Clusters. *Phys. Rev. Lett.* **1997**, *79* (24), 4778–4781. https://doi.org/10.1103/PhysRevLett.79.4778.

(68) Wang, C.; Wang, B.; Okunishi, M.; Roeterdink, W. G.; Ding, D.; Zhu, R.; Prümper, G.; Shimada, K.; Ueda, K. Ion-Ion Coincidence Imaging of Dissociative Ionization Dynamics of Formic Acid in Intense Laser Fields. *Chem. Phys.* **2014**, *430*, 40–46. https://doi.org/10.1016/j.chemphys.2013.12.003.

(69) Huet, T. R.; Pursell, C. J.; Ho, W. C.; Dinelli, B. M.; Oka, T. Infrared Spectroscopy and Equilibrium Structure of H2O +(X̃2B1). *J. Chem. Phys.* **1992**, *97* (9), 5977–5987. https://doi.org/10.1063/1.463735.

(70) Liu, D.; Zhang, C.; Hao, X.; Xue, X.; Gong, M.; Zhang, S.; Zhou, J.; Kong, C.; Yang, Z.; Ren, X.; Yang, T. On-the-Fly Nonadiabatic Molecular Dynamics Reveals Dissociation Mechanisms of Multiply Charged Molecules. *Phys. Rev. Lett.* **2026**, *136* (12). https://doi.org/10.1103/c8yq-fzn5.

(71) Bogot, A.; Poline, M.; Ji, M. C.; Dochain, A.; Rosén, S.; Zettergren, H.; Schmidt, H. T.; Thomas, R. D.; Strasser, D. Unravelling Non-Adiabatic Pathways in the Mutual Neutralization of Hydronium and Hydroxide. *Nat. Chem.* **2025**, *17* (4), 541–546. https://doi.org/10.1038/s41557-025-01771-6.

(72) Sutherland, J. R.; Christensen, E. L.; Powers, N. D.; Rhynard, S. E.; Painter, J. C.; Peatross, J. High Harmonic Generation in a Semi-Infinite Gas Cell. *Opt. Express* **2004**, *12* (19), 4430. https://doi.org/10.1364/OPEX.12.004430.

(73) Brichta, J. P.; Wong, M. C. H.; Bertrand, J. B.; Bandulet, H. C.; Rayner, D. M.; Bhardwaj, V. R. Comparison and Real-Time Monitoring of High-Order Harmonic Generation in Different Sources. *Phys. Rev. A* **2009**, *79* (3). https://doi.org/10.1103/PhysRevA.79.033404.

(74) Kandhasamy, D. M.; Albeck, Y.; Jagtap, K.; Strasser, D. 3D Coincidence Imaging Disentangles Intense Field Double Detachment of SF6-. *Journal of Physical Chemistry A* **2015**, *119* (29), 8076–8082. https://doi.org/10.1021/acs.jpca.5b04101.

(75) Urbain, X.; Bech, D.; Van Roy, J. P.; Géléoc, M.; Weber, S. J.; Huetz, A.; Picard, Y. J. A Zero Dead-Time Multi-Particle Time and Position Sensitive Detector Based on Correlation between Brightness and Amplitude. *Review of Scientific Instruments* **2015**, *86* (2). https://doi.org/10.1063/1.4908597.

(76) Lee, S. K.; Cudry, F.; Lin, Y. F.; Lingenfelter, S.; Winney, A. H.; Fan, L.; Li, W. Coincidence Ion Imaging with a Fast Frame Camera. *Review of Scientific Instruments* **2014**, *85* (12). https://doi.org/10.1063/1.4903856.

(77) Shahi, A.; Albeck, Y.; Strasser, D. Simultaneous 3D Coincidence Imaging of Cationic, Anionic, and Neutral Photo-Fragments. *Review of Scientific Instruments* **2018**, *89* (1). https://doi.org/10.1063/1.5004523.

(78) Livshits, E.; Baer, R. A Well-Tempered Density Functional Theory of Electrons in Molecules. *Physical Chemistry Chemical Physics* **2007**, *9* (23), 2932–2941. https://doi.org/10.1039/b617919c.

(79) Baer, R.; Livshits, E.; Salzner, U. Tuned Range-Separated Hybrids in Density Functional Theory. *Annu. Rev. Phys. Chem.* **2010**, *61*, 85–109. https://doi.org/10.1146/annurev.physchem.012809.103321.

(80) Livshits, E.; Granot, R. S.; Baer, R. A Density Functional Theory for Studying Ionization Processes in Water Clusters. *Journal of Physical Chemistry A* **2011**, *115* (23), 5735–5744. https://doi.org/10.1021/jp1057572.

(81) Shao, Y.; et. al., Advances in Molecular Quantum Chemistry Contained in the Q-Chem 4 Program Package. *Mol. Phys.* **2015**, *113* (2), 184–215. https://doi.org/10.1080/00268976.2014.952696.

(82) Tully, J. C. Molecular Dynamics with Electronic Transitions. *J. Chem. Phys.* **1990**, *93* (2), 1061–1071. https://doi.org/10.1063/1.459170.

Journal Name ARTICLE

View Article Online
DOI: 10.1039/D6CP00331A

(83) Shiozaki, T. BAGEL: Brilliantly Advanced General Electronic-Structure Library. *Wiley Interdiscip. Rev. Comput. Mol. Sci.* **2018**, *8* (1). https://doi.org/10.1002/wcms.1331.

(84) Finley, J.; Malmqvist, A.; Roos, B. O.; Serrano-Andres¨´, L.; Andres¨´, A. *The Multi-State CASPT2 Method a ˚ a a b*; 1998; Vol. 288.

(85) Vlaisavljevich, B.; Shiozaki, T. Nuclear Energy Gradients for Internally Contracted Complete Active Space Second-Order Perturbation Theory: Multistate Extensions. *J. Chem. Theory Comput.* **2016**, *12* (8), 3781–3787. https://doi.org/10.1021/acs.jctc.6b00572.

(86) Barbatti, M.; Ruckenbauer, M.; Plasser, F.; Pittner, J.; Granucci, G.; Persico, M.; Lischka, H. Newton-X: A Surface-Hopping Program for Nonadiabatic Molecular Dynamics. *Wiley Interdiscip. Rev. Comput. Mol. Sci.* **2014**, *4* (1), 26–33. https://doi.org/10.1002/wcms.1158.

(87) Park, J. W.; Shiozaki, T. On-the-Fly CASPT2 Surface-Hopping Dynamics. *J. Chem. Theory Comput.* **2017**, *13* (8), 3676–3683. https://doi.org/10.1021/acs.jctc.7b00559.

View Article Online
DOI: 10.1039/D6CP00331A

Data availability

The data supporting this study are available within the main text and the supplementary information (SI).